Domain Size Control in Self-Assembling Rod−Coil Block Copolymer and Homopolymer Blends

Yuefei Tao,[†,§] Bradley D. Olsen,[‡,§] Venkat Ganesan,[||] and Rachel A. Segalman*[,‡,§]

Department of Chemistry and Department of Chemical Engineering, University of California, Berkeley, California 94720, Materials Science Division, Lawrence Berkeley Laboratory, Berkeley, California 94720, and Department of Chemical Engineering, The University of Texas at Austin, Austin, Texas 78712

Received December 15, 2006; Revised Manuscript Received February 20, 2007

ABSTRACT: The addition of homopolymers to a self-assembling rod−coil block copolymer is demonstrated to be a flexible route toward domain size control. Molecular weight matched rod-like homopolymers interdigitate with the rod-blocks within their respective lamellae. As a result of the interdigitation, the coil blocks must rearrange to occupy more interfacial area resulting in an unprecedented decrease in domain spacing with increasing rod homopolymers. Conversely coil homopolymers were locally solubilized within the coil microdomain resulting in an increase of domain spacing with increasing coil homopolymers. The mechanisms of homopolymers solubilization are in qualitative agreement with predictions made by self-consistent mean-field theory (SCFT) calculations.

Introduction

The self-assembly of block copolymers provides an attractive means to control nanoscale morphology,[1,2] which allows for many useful applications including thermoplastic elastomers, adhesives, nanopatterned thin films,[3] and nanoscale templates.[4] Functional block copolymers containing helical proteins and semiconducting polymers blocks frequently do not follow traditional block copolymer phase diagrams[2] due to the rigid rod-like shape of the functional block. In the case of semiconducting polymers, the nanoscale domains that can result from self-assembly may be particularly useful in photovoltaics and light emitting applications where exciton separation or recombination occur at the interfaces between two polymers. Further, domain size control on the 10 nm length scale is crucial for optimizing device performance.[5−10]

The self-assembly of rod−coil diblock copolymers is controlled not only by the volume fraction of each block and the Flory−Huggins interaction between unlike blocks, but also by the tendency of the rod blocks to participate in anisotropic liquid crystalline interactions. The interplay between microphase separation and liquid crystallinity leads to phase behavior that is distinctly different from classical coil−coil diblock copolymers. For example, smectic, bicontinuous cubic, hexagonal, nematic, isotropic, strip, and puck phases have all been observed in both synthetic polymers and protein based systems.[11−17] In solution cast films even more unusual phases such as wavy lamellar, zigzag, and arrowhead morphologies have been seen.[18,19] Further, several protein-based oligomeric and polymeric rod−coil systems have been reviewed recently.[20−23] Recently, we demonstrated the synthesis of the weakly segregated rod−coil block copolymer that also follows polymeric scaling principles and used the accessible phase transitions to generate a phase diagram.[16,17] This model polymer system self-assembles into lamellar, nematic, and isotropic phases with changing coil volume fraction and temperature.

Block copolymer−homopolymer blends are an alternative method for controlling domain spacing and modifying morphology without additional synthesis.[1,24] In traditional coil−coil block copolymer systems, the solubilization of homopolymer chains into the block copolymer is controlled by the Flory interaction parameter, the grafting density (number of grafted chains per unit of area), and the molecular weights of the homopolymer and block copolymer.[25] The simplest and most studied case is when the homopolymer is chemically identical to one of the blocks. Depending primarily on the ratio of the block copolymer to the homopolymer molecular weights, the coil homopolymers may be uniformly distributed in the nanodomain resulting in stretching of the coil block (wet brush), or distributed primarily in the center of the nanodomain (dry brush) (both of which result in an increase in domain spacing), or macrophase separated from the block copolymer.[26−29] Conversely, when one of the blocks is crystallizable, the strong stretching of chains within the semicrystalline domain is relaxed upon addition of a semicrystalline homopolymer resulting in an overall reduction of domain spacing.[30]

The blending of a liquid crystalline rod−coil block copolymer with a rod homopolymer and/or a coil homopolymer is complicated by the anisotropic interactions and liquid crystalline behavior of the rod block. Since dispersity in rod length leads directly to interfacial broadening, it is expected that rod homopolymers will only be easily incorporated if they match the rod-block in size. Further, it is expected that rod homopolymers will align with the rod blocks. This greatly limits the morphologies available and introduces the possibility of interdigitation within a rod lamellar domain.

In this paper, we investigate the self-assembled structures in rod−coil block copolymers blended with rod, coil, or rod and coil homopolymers. The unusual stability of the lamellar phase in this system allows it to persist even with large amounts of homopolymer incorporated. The lamellar period varies based on the mechanism of homopolymer solubilization. Experimental results of lamellar spacing and microdomain structure are compared with predictions made by a self-consistent mean-field theory (SCFT), and a good agreement is found.

* Corresponding author. E-mail: segalman@berkeley.edu.
[†] Department of Chemistry, University of California, Berkeley.
[‡] Department of Chemical Engineering, University of California, Berkeley.
[§] Materials Science Division, Lawrence Berkeley Laboratory.
[||] Department of Chemical Engineering, The University of Texas at Austin.

10.1021/ma062876h CCC: $37.00
Published on Web 04/04/2007

Table 1. Block Copolymer PPV-*b*-PI and hPPV and hPI

polymer	PPV M_n (g/mol)[a]	PI M_n (g/mol)[b]	φ_{PI}	M_w/M_n
PPV-*b*-PI	3400	7100	0.70	1.09
hPPV	3400	0	0	1.17
hPI	0	7000	1.0	1.04

[a] Measured by NMR. [b] Measured by GPC.

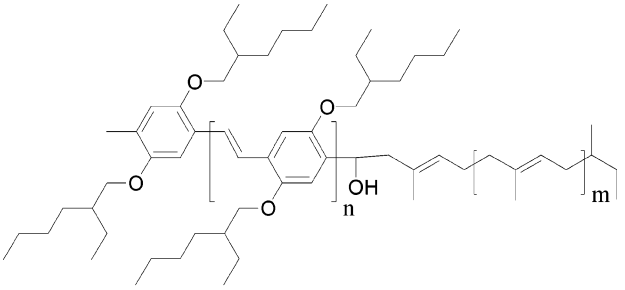

PPV-*b*-PI

Figure 1. Chemical structure of poly(2,5-di(2′-ethylhexyloxy)-1,4-phenylenevinylene-*block*-1,4-isoprene) (PPV-*b*-PI).

Experimental Methods

Materials. Materials were synthesized as previously described.[16] Table 1 summarizes characteristics of the homopolymers and block copolymer samples used in this work. Blends of homopolymers and block copolymers were prepared by first dissolving a predetermined amount of poly(2,5-di(2′-ethylhexyloxy)-1,4-phenylenevinylene-*block*-1,4-isoprene) (PPV-*b*-PI) (Figure 1) and poly(2,5-di(2′-ethylhexyloxy)-1,4-phenylenevinylene) homopolymer (hPPV) and/or poly(1,4-isoprene) homopolymer (hPI) in toluene and then by slowing evaporating the solvent at room temperature. The ternary mixtures were prepared along the isopleth line so that overall volume fractions of hPPV and hPI are kept equal, regardless of the volume fraction of PPV-*b*-PI block copolymer. The dried samples were annealed under vacuum for 48 h at 80 °C, a temperature within the lamellar phase but about the PPV melting temperature.[16,31] Small and wide-angle X-ray scattering (SAXS and WAXS) experiments were performed on beamline 1−4 of the Stanford Synchrotron Radiation Laboratory (SSRL) configured with an X-ray wavelength of 1.488 Å and focused to a spot size of 0.5 mm diameter. All measurements were taken with a sample cell temperature of 40 °C to ensure constant conditions during the measurement. Samples for transmission electron microscopy (TEM) were prepared by spin-coating films of 100 nm thickness from 1% toluene solution onto silicon nitride windows. The films were annealed under vacuum at 80 °C for 12 h and then cooled to room temperature. For transmission electron microscopy, films were exposed to osmium tetraoxide vapor for 4 h and then examined at 200 kV in the bright-field mode of a JEOL 200 CX microscope at the National Center for Electron Microscopy.

Results and Discussion

PPV-*b*-PI rod−coil block copolymers with coil fractions less than 0.85 exhibit lamellar structures[16] as demonstrated by a typical SAXS curve for the neat block copolymer in Figure 2a. The lamellar structure is indicated by high order peaks at multiples of q^* and is confirmed by microscopy shown in Figure 3a. Transmission electron micrographs obtained for samples stained with OsO_4 have dark PI domains and bright PPV lamellae. The neat PPV-*b*-PI block copolymer (Figure 3a) has grains of lamellae oriented both parallel and perpendicular to the plane of view similar to those previously observed.[16] Lamellae oriented perpendicular to the points of view appear as alternating light and dark stripes whereas lamellae oriented parallel to the plane of view appear as solid gray regions. The lamellar edges near the boundary of the parallel regions were revealed by imaging with a large tilt angle which indicates the lamellar nature of the grains.

Solubilization of Rod Homopolymers into Rod—Coil Block Copolymer. The solubilization of rod homopolymers into the rod−coil block copolymer is complicated by the anisotropic liquid crystalline interactions between the rod blocks. Rod containing lamellae are composed of rods with their long axes either perpendicular or at some angle from the block copolymer interface.[16] Additional rod homopolymer must be incorporated into this liquid crystalline structure, most likely by interdigitation with the block copolymer rods. Changes in the rod lamellar width would require reorientation of the rod tilt axis with respect to the block copolymer interface. TEM studies, as seen in Figure 3b, indicate that no macrophase separation is occurring so the rod is being incorporated into the microphase structure. Further, the addition of rod homopolymer does not perceptibly change the rod lamellar width indicating that the rod is incorporated in the liquid crystalline structure of the rod lamellae. These interdigitated lamellae, however, appear to have non-constant lamellar width, as indicated by waviness in the TEM image. The PPV liquid crystallinity is also disrupted by the addition of rod−homopolymer, as observed through the broadening of the rod−rod spacing (peak at 6.3 nm^{-1}, indicating a lateral rod spacing of 0.99 nm, as seen in Figure 4a).[16] This peak increases in width (full-width, half-maximum) from 0.17 to 0.23 nm^{-1} as the homopolymer fraction is raised to 40%.

The effect of the rod homopolymer on domain structure is most easily seen via SAXS, as shown in Figure 2a. SAXS also indicates that there is no macrophase separation (as indicated by the lack of q^{-4} scaling at low q range[32]) for the entire range of homopolymer fractions (0−40% homopolymer). With increasing fraction of rod homopolymer, however, the position of the q^* peak (and higher order peaks) shifts unexpectedly to higher q indicating a shrinkage in domain spacing. As the rod homopolymer fraction is increased, the lamellar spacing monotonically decreases as shown in Figure 5a.

It is clear, therefore, that rod homopolymer is absorbed in the rod lamellae, as shown in Figure 6a. This increase of material in the rod-lamellae increases the interfacial area of the lamellae. As a result, the coils must rearrange to occupy the additional interfacial area. To satisfy constant volume constraints, the coil domain, therefore, must shrink in width. As a result, we observe constant rod lamellar width but a dramatic shrinkage in domain spacing.

Scaling theory can be used to estimate the effect of rod homopolymer interdigitation on domain size under the assumption that the block copolymers are strongly segregated. For a block copolymer coil fraction ϕ and a rod homopolymer fraction Φ, the number of rod homopolymer chains per block copolymer chain will be

$$X = \frac{\Phi}{(1-\Phi)(1-\phi)} \tag{1}$$

If the rod homopolymer interdigitates with the rod-blocks, the width of rod nanodomains will not change. However, because the volume of the coil nanodomains is conserved in the strong segregation limit, the shrinkage of these nanodomains is given by

$$D'_{coil} = \frac{D_{coil}}{1+X} \tag{2}$$

For strongly segregated lamellar rod−coil block copolymers

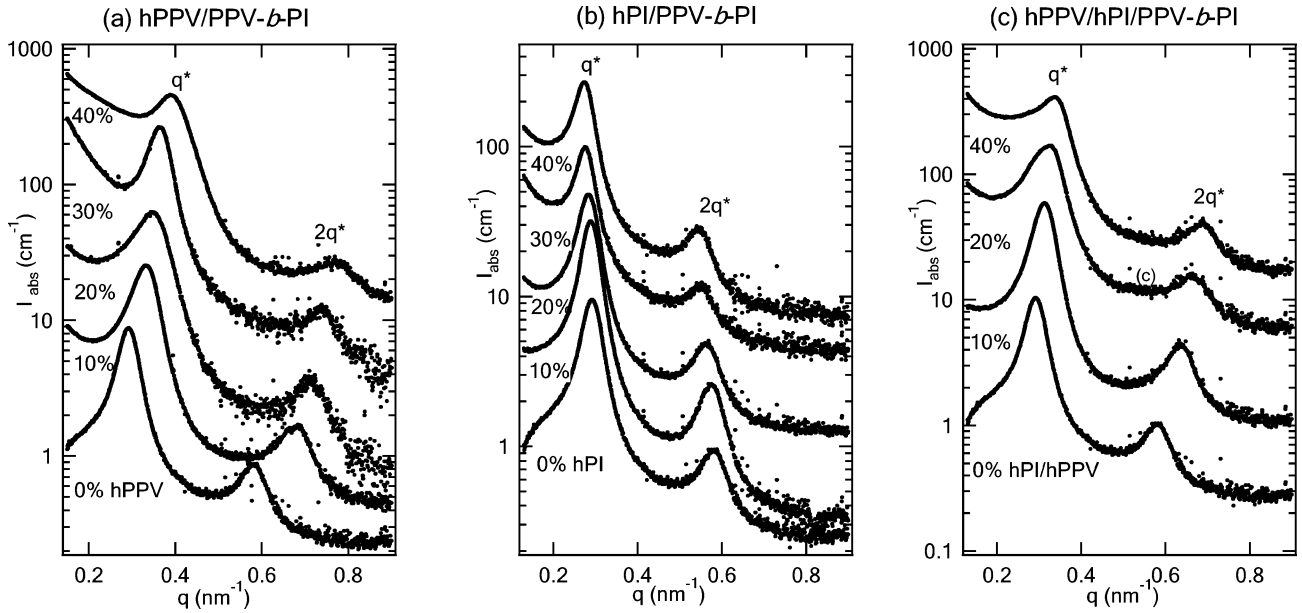

Figure 2. SAXS profiles taken at 40 °C for all blends demonstrate peaks at integer multiples of q indicating a lamellar structure. Digits within the plots indicate homopolymer fraction. The curves have been offset for clarity via a multiplicative factor. (a) For the addition of rod-homopolymer to a rod−coil block copolymer (hPPV/PPV-*b*-PI binary blends), the position of q^* and $2q^*$ shifts to higher q with increasing the fraction of rod homopolymer, indicating a shrinkage of domain spacing. (b) For the addition of coil polymer (hPI/PPV-*b*-PI binary blends), the postion of q^* and $2q^*$ shifts to lower q with increasing the fraction of coil homopolymer, indicating a swelling of domain spacing. (c) hPPV/hPI/PPV-*b*-PI ternary blends, the position of q^* and $2q^*$ shifts to higher q with increasing the fraction of rod/coil homopolymer, indicating an overall shrinkage of domain spacing.

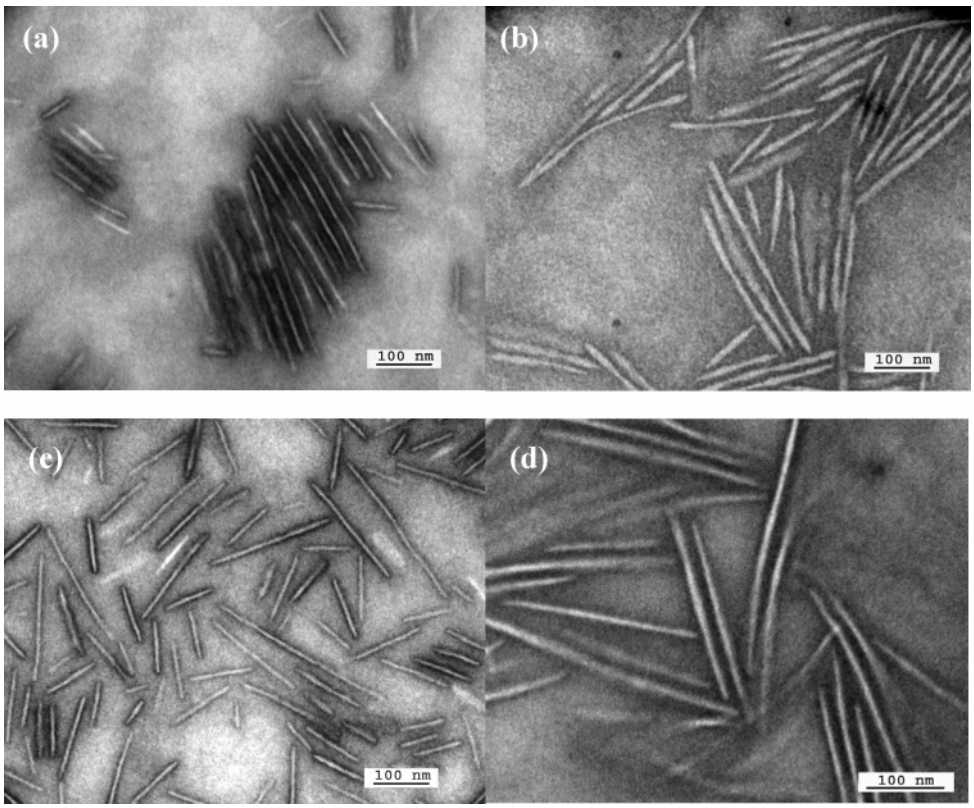

Figure 3. Transmission electron micrographs of rod−coil block copolymer/homopolymer blends stained with OsO_4. All structures are lamellar. Uniform colored areas are lamellae oriented roughly parallel to the plane of view (lamellar fringes are visible upon tilting not shown). Key: (a) neat PPV-*b*-PI, (b) 40% volume fraction of hPPV blend with PPV-*b*-PI , (c) 40% volume fraction of hPI blend with PPV-*b*-PI, and (d) 40% volume fraction of hPPV/hPI with block copolymer.

both the rod and coil nanodomains are predicted to scale linearly with molecular weight, so the new domain spacing is given by

$$D' = Na\cos\theta\left((1-\phi)+\frac{\phi}{1+X}\right) \qquad (3)$$

where N is the total number of repeat units in the block copolymer, a is the statistical segment length of the rod polymer, and θ is the angle between the rod director and the lamellar normal. The scaling theory calculation, as plotted in Figure 5a, overpredicts the shrinkage of the coil block primarily because

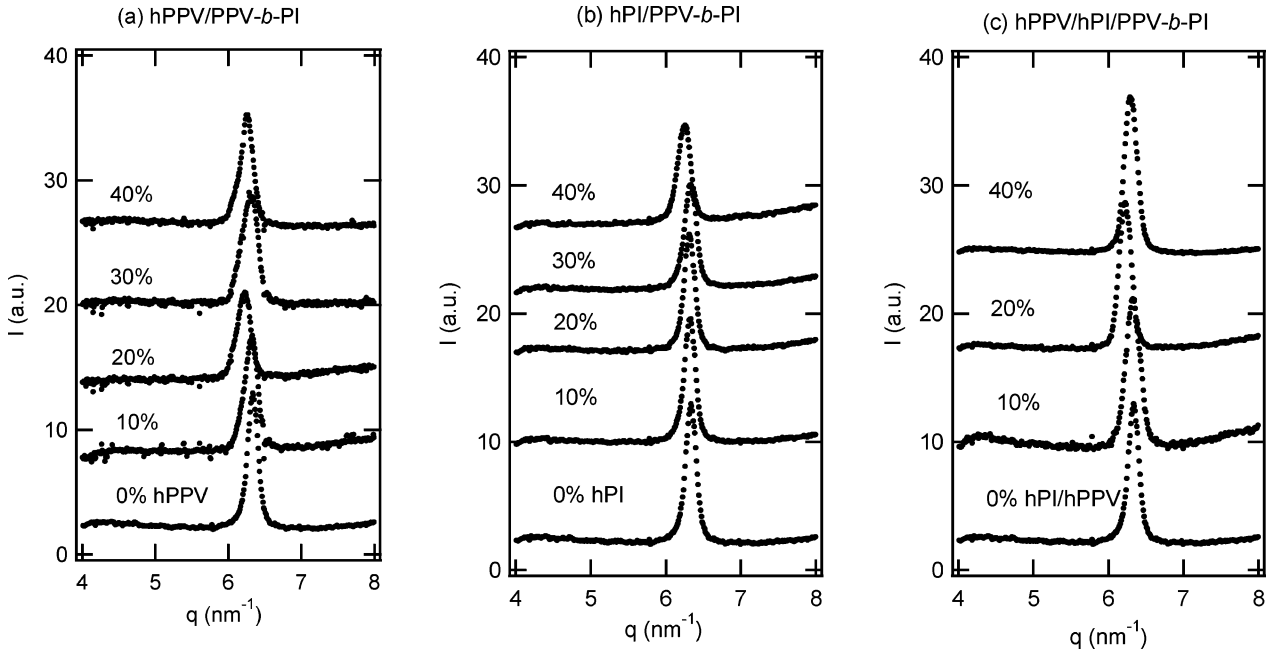

Figure 4. Wide-angle X-ray scattering profiles taken at 40 °C for (a) hPPV/PPV-*b*-PI binary blends. As homopolymer fraction increases, the primary peak broadens from a full width, half-maximum of 0.17−0.23 nm^{-1}) indicating that the additional rods introduce slight disorder within the smectic stack. (b) hPI/PPV-*b*-PI binary blends. The primary peak has no perceptible change with increasing fraction of coil homopolymers, indicating that the coil homopolymers simply swell the coil lamellae leaving the rest of the structure unchanged. (c) hPPV/hPI/PPV-*b*-PI ternary blends. The primary peak around 6.3 nm^{-1} corresponds to the spacing between rod blocks. The digits indicate the volume percent of homopolymers in the mixture.

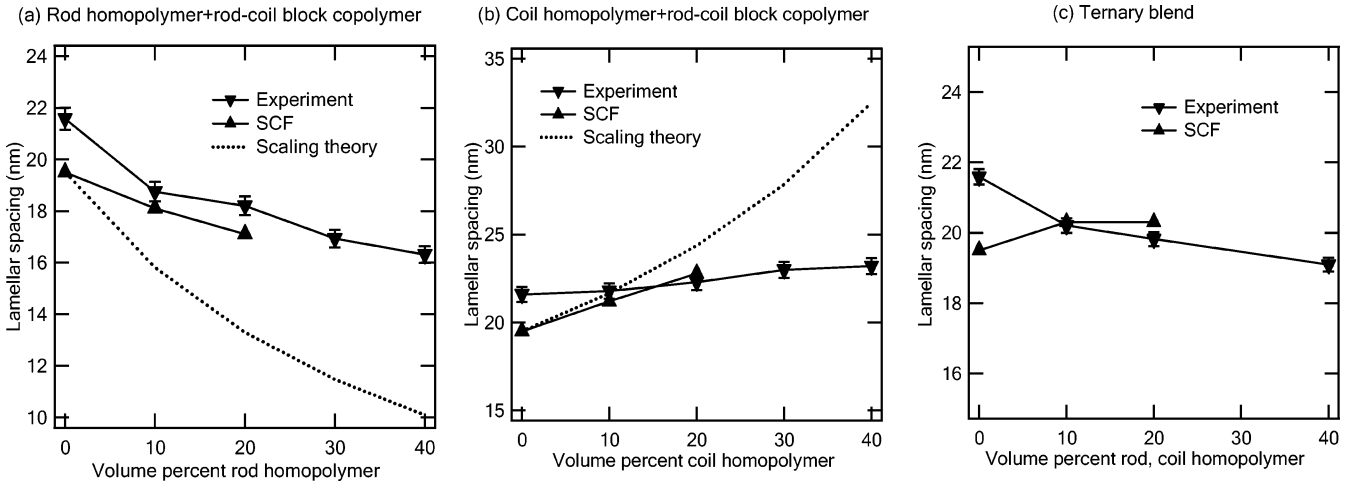

Figure 5. Effect of homopolymer in rod−coil block copolymer lamellar spacing (a) additional rod homopolymer, (b) additional coil homopolymer, and (c) ternary blends of rod homopolymer, coil homopolymer, and rod−coil diblock copolymer. Both SCF and scaling theory predict that the addition of rod to the block copolymer results in the experimentally observed reduction in lamellar spacing while the addition of coil homopolymer is expected to result in swelling of the coil domain.

it does not account for interfacial broadening that occurs in the weakly segregated limit of the experiment.

SCFT simulation results are also consistent with interdigitation, as shown in Figure 7b. These models suggest that the rod nanodomains will maintain roughly constant width while the overall domain spacing decreases with the addition of rod homopolymer, as shown in Figure 5a. These predictions are in better agreement with experiment than scaling theory at low volume fractions of homopolymer. At high concentrations of rod homopolymer, however, the SCFT predictions suggest that some of the rod homopolymer will become isolated into the middle of the rod domain. This macrophase separation is not seen in experiments, so it becomes impossible to compare SCFT predictions and experiments at larger volume fractions of homopolymer.

At low homopolymer loadings, SCFT suggests that the homopolymer rods uniformly span the entire width of the rod domain. As the rod homopolymer interdigitates with the rod blocks of the block copolymer, it pushes apart of the rod blocks. As a result of the interdigitation, the coil blocks must rearrange to occupy more interfacial area which results in an unprecedented decrease in domain spacing with increasing rod homopolymer. This behavior is obviously a result of liquid crystalline interactions between rod which dramatically affect the incorporation mechanism of liquid crystalline homopolymer into the self-assembly.

Solubilization of Coil Homopolymers into Rod−Coil Block Copolymer. The solubilization of coil homopolymers into the rod−coil block copolymer is simpler than that of rod homopolymers since there is no liquid crystalline constraint within the

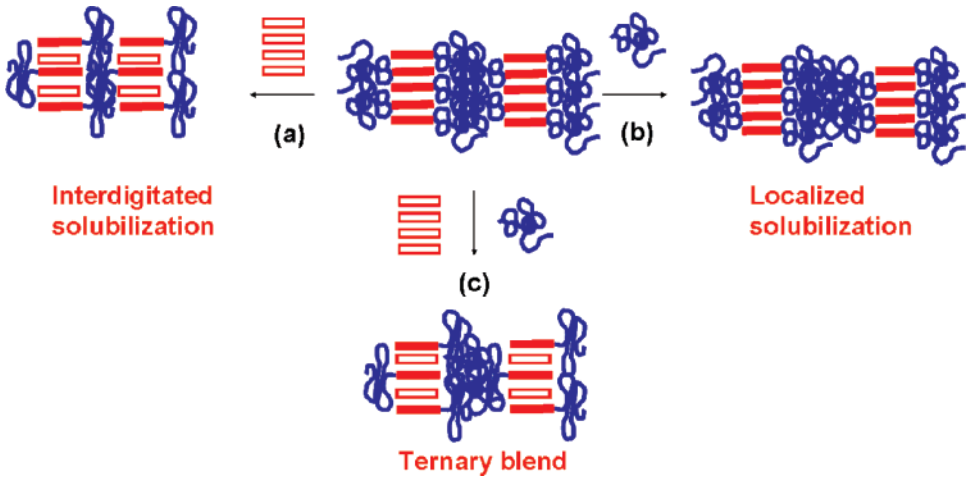

Figure 6. (a) Rod homopolymers interdigitate with the rod blocks of the rod−coil block copolymers resulting in increasing interfacial area and causing the coil blocks to rearrange. This results in an overall decrease in lamellar spacing. (b) Coil homopolymers swell the coil blocks of the rod−coil block copolymers resulting in increasing lamellar spacing. (c) Ternary blend of rod and coil homopolymers with rod−coil block copolymers has a combination of the two effects.

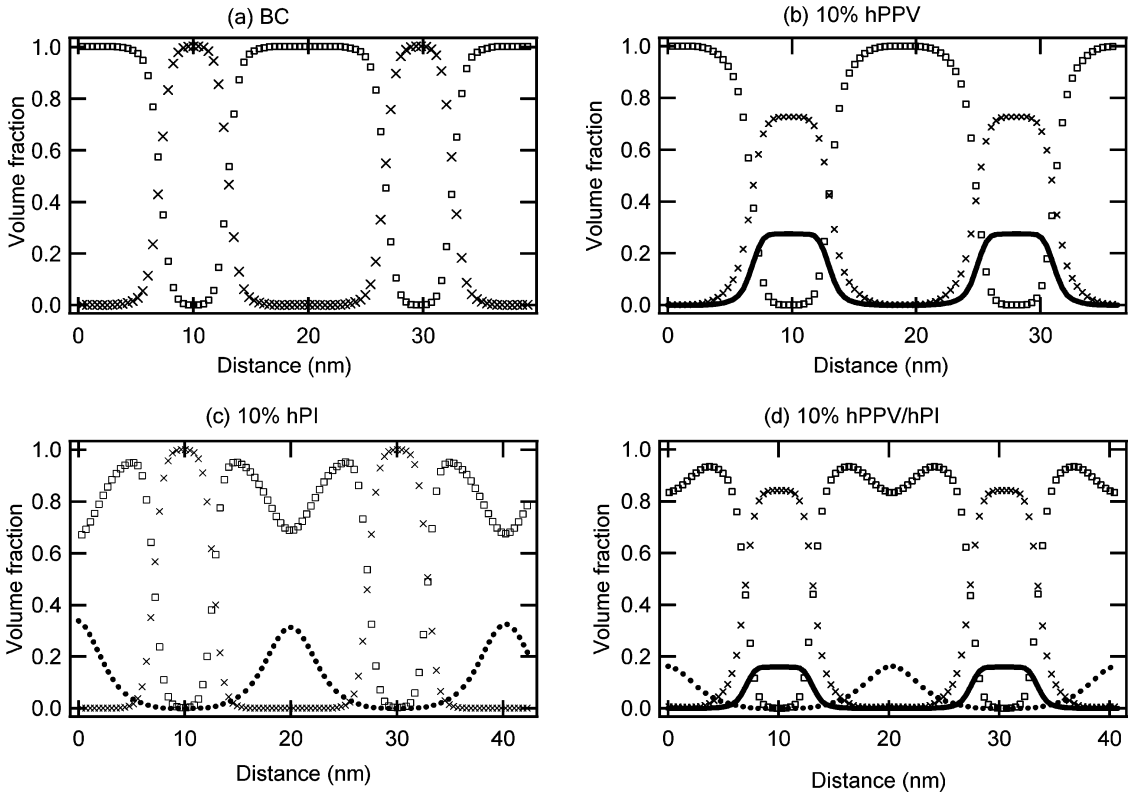

Figure 7. SCF simulation results for (a) neat PPV-*b*-PI, (b) hPPV/PPV-*b*-PI binary blends with10% hPPV, (c) hPI/PPV-*b*-PI binary blends with 10% hPI, and (d) hPPV/hPI/PPV-*b*-PI ternary blends with 10% hPPV/hPI. Key: (□) volume fraction of coil block; (×) rod block, (—) rod homopolymer; (●) coil homopolymer. All at $\chi N_{RC} = 24.45$, $\mu N_{RC} = 43.2$, and $N = 150$.

coil lamellae. TEM images (Figure 3c) of coil-swollen blends are almost indistinguishable from the neat block copolymer demonstrating very straight lamellae. As expected, the rod lamellar width and rod−rod spacings (as observed through WAXS shown in Figure 4b) are unchanged as coil homopolymer is added. SAXS, however, demonstrates that the location of the q^* and $2q^*$ peaks shift to lower q as the amount of hPI increases indicating the expected swelling of the microphases. The continuous increase in domain spacing with coil fraction is seen in Figure 5b. Under the assumption that the rod packing and nanodomain size remain unchanged, the increase in domain spacing can be calculated by simple volumetric arguments. For a coil homopolymer fraction Φ, the swollen domain spacing is

$$D' = \frac{Na\cos\theta}{1-\Phi} \tag{4}$$

This curve is plotted as a dotted line in Figure 5b. This swelling behavior upon addition of coil homopolymer follows most predictions for swelling of coil−coil block copolymers and our own SCFT predictions shown in Figure 7c. In agreement with experimental results, both SCFT predictions and scaling theory calculations predict that the coil domains are increasingly swollen with homopolymer but the rod domains remain unchanged (as shown in Figure 6b).

It is interesting to note that the domain spacing of the block copolymer blends increases much more slowly with increasing

coil fraction than that of pure block copolymers with equivalent coil fractions. For example, a block copolymer with a similarly sized rod and $\Phi_{PI} = 42\%$[16] has a domain spacing of about 14 nm, but a block copolymer with $\Phi_{PI} = 70\%$ blended with enough rod homopolymer to bring the total coil content to 42% (40% homopolymer) has a domain spacing of approximately 17 nm. Increasing coil fraction results in a relatively slow increase of domain spacing for the blend compared with the neat block copolymers: at 20% rod homopolymer, the domain spacing is about 18 nm while the domain spacing of a block copolymer with a similar coil fraction ($\Phi_{PI} = 59\%$) is 17 nm. Similarly, swelling with coil results in a smaller domain spacing increase than increasing coil fraction; at 20% coil homopolymer a domain spacing of 22 nm is observed, while a block copolymer with an equivalent coil fraction ($\Phi_{PI} = 82\%$) has a domain spacing of 29 nm. This result is contrary to the prediction of the scaling theory that suggests domain spacing should be a function of the total volume fractions only. The experimental results suggest that rod or coil homopolymer insertion result in chain rearrangements to minimize the free energy.

Solubilization of Rod and Coil Homopolymers into Rod−Coil Block Copolymer. Rod homopolymers are interdigitated within the rod phase and coil homopolymers are locally solubilized within the coil phase. When both rod and coil homopolymers are added, these two effects compete allowing for control over lamellar spacing as shown in Figures 2c and 5c. The effects of coil stretching to accommodate additional rod interfacial area can be mediated by adding more coil homopolymers. In this case as hPPV/hPI content is increased, the lamellar spacing decreases, indicating that at equal volume fractions of rod and coil homopolymers, the rod's effect is larger than the coil as illustrated in Figure 6a.

Similarly, SCFT simulations, shown in Figure 7d, confirm that in ternary blends the rod homopolymer will still interdigitate within the rod nanodomains, and the coil homopolymer will still swell the coil nanodomains. However, while the simulations predict a small increase in domain spacing relative to the neat block copolymer, the experimental results show a small decrease in domain spacing. This slight discrepancy is within the limits of the prediction most likely due to both inaccuracies in the value of Flory−Huggins parameter(χ) used and nonidealities of mixing. As a result, SCFT overpredicts the rate of change in domain spacing with homopolymer addition in all cases, but more for the coil block. As a result when the two homopolymers are added in equal amounts to the block copolymer, the result is an overall slight increase in domain spacing while experiments display an incremental decrease.

This phenomenon is sketched in Figure 6c for the ternary mixtures, the rod homopolymers tend to interdigitate within the rod blocks and the coil homopolymers tend to be locally solubilized into the coil lamellar microdomains. The interdigitated solubilization causes the contraction of the coil block domains and the locally solubilization causes the expansions of the coil block domains. At equal rod−coil volume fractions, the contraction caused by the interdigition is larger than the expansion caused by coil swelling. For example, at 20% volume fraction of homopolymers, the rod binary blend has 16% contraction while the coil binary blend has only 3.2% expansion relative to the neat block copolymer. As expected, the lamellar spacing can be controlled by change the volume ratio of the rod and coil homopolymers.

Conclusions

Self-assembly of model systems of rod−coil block copolymers PPV-b-PI blended with rod hPPV, coil hPI, or rod and coil homopolymers was investigated as a function of homopolymer content at 40 °C. As sketched in Figure 6a, rod homopolymers interdigitate with the rod-blocks within their respective lamellae. As a result of the interdigitation, the coil blocks must rearrange to occupy more interfacial area. This results in an unprecedented decrease in domain spacing with increasing rod homopolymer. Conversely, when coil homopolymers are incorporated, they are locally solubilized within the coil microdomain resulting in an increase of domain spacing with increasing coil homopolymer. For the ternary mixtures, the rod homopolymers tend to interdigitate with the rod blocks and the coil homopolymers tend to be locally solubilized into the coil lamellar microdomains. The interdigitated solubilization causes the contraction of the coil block domains and the locally solubilization causes the expansions of the coil block domains. The mechanism of homopolymer solubilization is in qualitative agreement with predictions made by a self-consistent mean-field theory.

Acknowledgment. We gratefully acknowledge support from the Department of Energy Office of Basic Energy Sciences through the Plastic Electronics Program at Lawrence Berkeley National Lab (LBNL) and an NSF-CAREER Award. VG acknowledges support from Robert A. Welch Foundation. B.D.O. gratefully acknowledges a graduate fellowship from the Fannie and John Hertz Foundation. SAXS and WAXS experiments were performed at the Stanford Synchrotron Radiation Laboratory, a national user facility operated by Stanford University and TEM experiments were performed at the National Center for Electron Microscopy at LBNL, both supported by the Department of Energy, Office of Basic Energy Sciences. We also gratefully acknowledge helpful discussions with Dr. Ed Feng and assistance with TEM from W. R. Hudson.

Appendix

Self-Consistent Field Theory. To model the swelling of rod−coil block copolymers with rod and coil hompolymers, we have extended the self-consistent field theory model of Pryamitsyn and Ganesan[34] to include rod and coil hompolymers. The coil homopolymer and coil block of the block copolymer are modeled as Gaussian coils with statistical segment length b and segmental volume ρ_o^{-1}. The rod homopolymer and rod block of the block copolymer are modeled as rigid rods of statistical segment length a such that the volume of a rod segment is also ρ_o^{-1}. In this model, we define three order parameters: the total coil density, ρ_C; the total rod density, ρ_R; and the orientational order parameter, $\mathbf{S}$.

$$\hat{\rho}_C(\mathbf{r}) = \sum_{\alpha=1}^{M_C}\int_0^{N_C} ds\, \delta(\mathbf{r} - \mathbf{R}_\alpha(s)) + \sum_{\alpha=1}^{M_{RC}}\int_0^{\phi N_{RC}} ds\, \delta(\mathbf{r} - \mathbf{R}_\alpha(s)) \quad \text{(A1)}$$

$$\hat{\rho}_R(\mathbf{r}) = \sum_{\alpha=1}^{M_R}\int_0^{N_R} ds\, \delta(\mathbf{r} - (\mathbf{R}_\alpha(0) + as\mathbf{u}_\alpha)) + \sum_{\alpha=1}^{M_{RC}}\int_0^{N_{RC}(1-\phi)} ds\, \delta(\mathbf{r} - (\mathbf{R}_\alpha(N_{RC}\phi) + as\mathbf{u}_\alpha)) \quad \text{(A2)}$$

$$\hat{\mathbf{S}}(\mathbf{r}) = \sum_{\alpha=1}^{M_R}\int_0^{N_R} ds\, \delta(\mathbf{r} - (\mathbf{R}_\alpha(0) + as\mathbf{u}_\alpha))\left[\mathbf{u}_\alpha\mathbf{u}_\alpha - \frac{\mathbf{I}}{3}\right] + \sum_{\alpha=1}^{M_{RC}}\int_0^{N_{RC}(1-\phi)} ds\, \delta(\mathbf{r} - (\mathbf{R}_\alpha(N_{RC}\phi) + as\mathbf{u}_\alpha))\left[\mathbf{u}_\alpha\mathbf{u}_\alpha - \frac{\mathbf{I}}{3}\right] \quad \text{(A3)}$$

where ϕ is the coil volume fraction of the block copolymer, M is the total number of molecules, N is the number of volumetric repeat units per molecule, $\mathbf{R}$ is the molecular path, and $\mathbf{u}$ is the rod orientation vector. Subscripts R, C, and RC indicate rod homopolymer, coil homopolymer, and rod−coil block copolymer, respectively.

The simulation is performed in the canonical ensemble. Similarly to the original model, the Hamiltonian contains three terms due to the harmonic stretching energy of the chain, the Flory−Huggins interaction, and the Maier−Saupe interaction:

$$H_{CS} = \frac{3}{2b^2}\left[\sum_{\alpha=1}^{M_C}\int_0^{N_C} ds \left|\frac{d\mathbf{R}_\alpha(s)}{ds}\right|^2 + \sum_{\alpha=1}^{M_{RC}}\int_0^{\phi N_{RC}} ds \left|\frac{d\mathbf{R}_\alpha(s)}{ds}\right|^2\right] \tag{A4}$$

$$H_{FH} = -\frac{\chi}{4\rho_o}\int_V d\mathbf{r}\,[\hat{\rho}_C(\mathbf{r}) - \hat{\rho}_R(\mathbf{r}) - (2\Phi - 1)\rho_o]^2 \tag{A5}$$

$$H_{MS} = -\frac{\mu}{2\rho_o}\int_V d\mathbf{r}\,\hat{\mathbf{S}}(\mathbf{r}):\hat{\mathbf{S}}(\mathbf{r}) \tag{A6}$$

where Φ is the total coil fraction and Φ_i is the coil fraction of a single component in the blend such that

$$\Phi = \bar{\Phi}_C + \phi\bar{\Phi}_{RC} \tag{A7}$$

After a Hubbard−Stratanovich transformation to a field-theoretic model, the resulting partition function is

$$Z \propto \int Dw \int D\pi \int D\mathbf{M} \exp \left[-\frac{C}{\chi N_{RC}}\int_V d\mathbf{x}\, w^2 + iC\int_V d\mathbf{x}\,\pi - C(2\Phi - 1)\int_V d\mathbf{x}\; w \right. \\ \left. -\frac{C}{2\mu N_{RC}}\int_V d\mathbf{x}\,\mathbf{M}:\mathbf{M} + M_C \ln Q_C + M_R \ln Q_R + M_{RC} \ln Q_{RC}\right] \tag{A8}$$

and the single chain partition functions, Q, for molecules interacting with the spatially dependent fields w, π, and $\mathbf{M}$ are given by

$$Q_C = \int D\mathbf{R} \exp\left[-\frac{1}{4}\int_0^{\alpha_C} dt \left|\frac{d\mathbf{R}}{dt}\right|^2 + \int_0^{\alpha_C} dt\,(w(\mathbf{R}(t)) - i\pi(\mathbf{R}(t)))\right] \tag{A9}$$

$$Q_R = \int_V d\mathbf{x} \int d\mathbf{u} \exp\left[\int_0^{\alpha_R} dt \left[-i\pi(\mathbf{x} + \beta t\mathbf{u}) - w(\mathbf{x} + \beta t\mathbf{u}) + M(\mathbf{x} + \beta t\mathbf{u}):\left(\mathbf{uu} - \frac{\mathbf{I}}{3}\right)\right]\right] \tag{A10}$$

$$Q_{RC} = \int D\mathbf{R} \int d\mathbf{u} \exp\left[-\frac{1}{4}\int_0^{\phi} dt \left|\frac{d\mathbf{R}}{dt}\right|^2 + \int_0^{\phi} dt\,[w(\mathbf{R}(t)) - i\pi(\mathbf{R}(t))]\right] \times \exp\left[\int_0^{(1-\phi)} dt \left[-i\pi(\mathbf{R}(\phi) + \beta t\mathbf{u}) - w(\mathbf{R}(\phi) + \beta t\mathbf{u}) + \mathbf{M}(\mathbf{R}(\phi) + \beta t\mathbf{u}):\left(\mathbf{uu} - \frac{\mathbf{I}}{3}\right)\right]\right] \tag{A11}$$

where the new equations have been nondimensionalized using the spatial and chain length coordinates x and t

$$x = \frac{r}{b\sqrt{\frac{N_{RC}}{6}}} \tag{A12}$$

$$t = \frac{s}{N_{RC}} \tag{A13}$$

The parameters α_C and α_R are defined as the number of repeat units in the coil and rod homopolymer relative to the block copolymer

$$\alpha_C = \frac{N_C}{N_{RC}} \tag{A14}$$

$$\alpha_R = \frac{N_R}{N_{RC}} \tag{A15}$$

The parameter β is a length ratio related to the ratio between the rod length, L_R, and coil radius of gyration, $R_{g,C}$

$$\beta = \frac{aN_{RC}}{b\sqrt{\frac{N_{RC}}{6}}} = \frac{\phi^{0.5}}{1-\phi}\frac{L_R}{R_{g,C}} \tag{A16}$$

The constant C is a dimensionless segment density,

$$C = \frac{\rho_o\left(b\sqrt{\frac{N_{RC}}{6}}\right)^3}{N_{RC}} \tag{A17}$$

The partition functions for the coil homopolymer and rod−coil block copolymer may be reexpressed in terms of a chain propagator $q(\mathbf{x}, \alpha_C)$[35−37]

$$Q_C = \frac{1}{V}\int d\mathbf{x}\; q(\mathbf{x},\alpha_C) \tag{A18}$$

$$Q_{RC} = \frac{1}{V}\int d\mathbf{x} \int d\mathbf{u}\; q(\mathbf{x}, \phi) \exp\left[\int_0^{(1-\phi)} dt \left[-i\pi(\mathbf{R}(\phi) + \beta t\mathbf{u}) - w(\mathbf{R}(\phi) + \beta t\mathbf{u}) + \mathbf{M}(\mathbf{R}(\phi) + \beta t\mathbf{u}):\left(\mathbf{uu} - \frac{\mathbf{I}}{3}\right)\right]\right] \tag{A19}$$

where $q(\mathbf{x}, \alpha_C)$ solves the modified diffusion equation and initial condition

$$\frac{\partial}{\partial t}q(\mathbf{x},t) = \nabla^2 q(\mathbf{x},t) + q[w(\mathbf{x}) - i\pi(\mathbf{x})] \tag{A20}$$

$$q(\mathbf{x},0) = 1 \tag{A21}$$

and periodic boundary conditions are used. The volume fractions and orientational parameters can also be calculated for arbitrary fields

$$\Phi_C(\mathbf{x}) = \frac{\bar{\Phi}_C V}{\alpha_C Q_C}\int_0^{\alpha_C} dt\; q(\mathbf{x},t)q'(\mathbf{x},t) \tag{A22}$$

$$\Phi_R(\mathbf{x}) = \frac{\bar{\Phi}_R V}{\alpha_R Q_R} \int d\mathbf{u} \int_0^{\alpha_R} dt \exp\left[\int_0^{\alpha_R} dt' \begin{pmatrix} \pi(\mathbf{x}+\beta(t'-t)\mathbf{u}) - w(\mathbf{x}+\beta(t'-t)\mathbf{u}) \\ + M(\mathbf{x}+\beta(t'-t)\mathbf{u}):\left(\mathbf{uu}-\frac{\mathbf{I}}{3}\right) \end{pmatrix}\right] \quad \text{(A23)}$$

$$(\phi\Phi_{RC})(\mathbf{x}) = \frac{\bar{\Phi}_{RC} V}{Q_C} \int_0^{\phi} dt\, q(\mathbf{x},t) q'(\mathbf{x}, \phi - t) \quad \text{(A24)}$$

$$((1-\phi)\Phi_{RC})(\mathbf{x}) = \frac{\bar{\Phi}_{RC} V}{Q_R} \int d\mathbf{u} \int_0^{1-\phi} dt\, q(\mathbf{x}-\beta t\mathbf{u},\phi) \exp\left[\int_0^{1-\phi} dt' \begin{pmatrix} \pi(\mathbf{x}+\beta(t'-t)\mathbf{u}) - w(\mathbf{x}+\beta(t'-t)\mathbf{u}) \\ + M(\mathbf{x}+\beta(t'-t)\mathbf{u}):\left(\mathbf{uu}-\frac{\mathbf{I}}{3}\right) \end{pmatrix}\right] \quad \text{(A25)}$$

$$\mathbf{S}(\mathbf{x}) = \frac{\bar{\Phi}_R V}{\alpha_R Q_R} \int d\mathbf{u} \int_0^{\alpha_R} dt \left(\mathbf{uu}-\frac{\mathbf{I}}{3}\right) \exp\left[\int_0^{\alpha_R} dt' \begin{pmatrix} \pi(\mathbf{x}+\beta(t'-t)\mathbf{u}) - w(\mathbf{x}+\beta(t'-t)\mathbf{u}) \\ + M(\mathbf{x}+\beta(t'-t)\mathbf{u}):\left(\mathbf{uu}-\frac{\mathbf{I}}{3}\right) \end{pmatrix}\right] + \frac{\bar{\Phi}_{RC} V}{Q_R} \int d\mathbf{u} \int_0^{1-\phi} dt \left(\mathbf{uu}-\frac{\mathbf{I}}{3}\right) q(\mathbf{x}-\beta t\mathbf{u},\phi) \exp\left[\int_0^{1-\phi} dt' \begin{pmatrix} \pi(\mathbf{x}+\beta(t'-t)\mathbf{u}) - w(\mathbf{x}+\beta(t'-t)\mathbf{u}) \\ + M(\mathbf{x}+\beta(t'-t)\mathbf{u}):\left(\mathbf{uu}-\frac{\mathbf{I}}{3}\right) \end{pmatrix}\right] \quad \text{(A26)}$$

Solving for saddle-points of the partition function in the mean field approximation yields the self-consistent equations

$$\frac{2}{\chi N_{RC}} w(\mathbf{r}) = \Phi_C(\mathbf{r}) - \Phi_R(\mathbf{r}) - (2\Phi - 1) \quad \text{(A27)}$$

$$1 = \Phi_C(\mathbf{r}) + \Phi_R(\mathbf{r}) \quad \text{(A28)}$$

$$\frac{1}{\mu N_{RC}} \mathbf{M}(\mathbf{r}) = \mathbf{S}(\mathbf{r}) \quad \text{(A29)}$$

To solve these equations numerically, we use the pseudodynamical steepest descent algorithm developed by Fredrickson and co-workers[35,38] and previously used by Pryamitsyn and Ganesan.[34] According to this algorithm, an initial guess is used to seed the fields and calculate order parameters. From these order parameters a new set of fields is calculated, and the original fields are evolved according to pseudodynamical equations. Because we only performed calculations in one dimension, our simulations are limited to lamellar morphologies. The modified diffusion equation was solved using finite difference techniques. We used 75 lattice points in the t dimension and 400 in the x dimension such that dt and dx had approximately equal spatial extent. The configurational integral over rod orientation was evalued using Gaussian quadrature with 10 points in θ and 32 points in φ. Since PPV is strongly liquid crystalline at the temperatures of interest,[31] initial simulations were carried out using random w and π fields and a fully oriented **M** field to estimate the equilibrium microphase. The equilibrium lamellar domain spacing was chosen by minimizing the free energy.

Eight dimensionless groups govern the behavior of the rod/coil/rod−coil system: χN_{RC}, μN_{RC}, α_C, α_R, β, ϕ, Φ_R, and Φ_C. To facilitate direct comparisons between computation and experiment, quantitative estimates for all of these parameters were obtained from independent experiments. β, α_C, α_R, ϕ, Φ_R, and Φ_C can all be estimated based on density, molecular weight, and bond length data.[16] μN_{RC} was previously determined as a function of temperature using experiments on PPV hompolymers.[31] Using the volume of a single isoprene unit as a reference volume, $N_{RC} = 150$, $N_C = 46$, and $N_R = 104$. The value of χ used was estimated based on the ODT of neat block copolymers.[16,31] Referencing the experimental PPV-*b*-PI phase diagram to the theoretical phase diagram of Pramitsyn and Ganesan,[34] the ODT at a coil fraction of approximately 0.85 corresponds to a temperature of 60 °C and a χN of 24.45. The experimental N is 150, so χ is approximately 0.163.

References and Notes

(1) Hamley, I. W. *The Physics of Block Copolymers*. Oxford University Press: New York, 1998.
(2) Bates, F. S.; Fredrickson, G. H. *Phys. Today* **1999**, *52* (2), 32−38.
(3) Segalman, R. A. *Mater. Sci. Eng. R-Rep.* **2005**, *48*, (6), 191−226.
(4) Fasolka, M. J.; Mayes, A. M. *Annu. Rev. Mater. Res.* **2001**, *31*, 323−355.
(5) Milner, R. G.; Arias, A. C.; Stevenson, R.; Mackenzie, J. D.; Richards, D.; Friend, R. H.; Kang, D. J.; Blamire, M. *Mater. Sci. Technol.* **2002**, *18*, 759−762.
(6) Moons, E. *J. Phys., Condens. Matter* **2002**, *14*, 12235−12260.
(7) Higgins, A. M.; Martin, S. J.; Thompson, R. L.; Chappell, J.; Voigt, M.; Lidzey, D. G.; Jones, R. A. L.; Geoghegan, M. *J. Phys., Condens. Matter* **2005**, *17*, 1319−1328.
(8) Voigt, M.; Chappell, J.; Rowson, T.; Cadby, A.; Geoghegan, M.; Jones, R. A. L.; Lidzey, D. G. *Org. Electron.* **2005**, *6* (1), 35−45.
(9) Ball, Z. T.; Sivula, K.; Frechet, J. M. J. *Macromolecules* **2006**, *39*, 70−72.
(10) Sivula, K.; Ball, Z. T.; Watanabe, N.; Frechet, J. M. J. *Adv. Mater.* **2006**, *18* (2), 206−210.
(11) Radzilowski, L. H.; Wu, J. L.; Stupp, S. I. *Macromolecules* **1993**, *26*, 879−882.
(12) Radzilowski, L. H.; Stupp, S. I. *Macromolecules* **1994**, *27*, 7747−7753.
(13) Radzilowski, L. H.; Carragher, B. O.; Stupp, S. I. *Macromolecules* **1997**, *30*, 2110−2119.
(14) Lee, M.; Cho, B. K.; Kim, H.; Zin, W. C. *Angew. Chem. Int. Ed.* **1998**, *37*, 638−640.
(15) Ryu, J. H.; Oh, N. K.; Zin, W. C.; Lee, M. *J. Am. Chem. Soc.* **2004**, *126*, 3551−3558.
(16) Olsen, B. D.; Segalman, R. A. *Macromolecules* **2005**, *38*, 10127−10137.
(17) Olsen, B. D.; Segalman, R. A. *Macromolecules* **2006**, *39*, 7078−7083.
(18) Chen, J. T.; Thomas, E. L.; Ober, C. K.; Hwang, S. S. *Macromolecules* **1995**, *28*, 1688−1697.
(19) Chen, J. T.; Thomas, E. L.; Ober, C. K.; Mao, G. P. *Science* **1996**, *273* (5273), 343−346.
(20) Gallot, B. *Prog. Polym. Sci.* **1996**, *21*, 1035−1088.
(21) Lee, M.; Cho, B. K.; Zin, W. C. *Chem. Rev.* **2001**, *101*, 3869−3892.
(22) Stupp, S. I. *Curr. Opin. Colloid Interface Sci.* **1998**, *3* (1), 20−26.
(23) Loos, K. M.-G. S. In *Supramolecular Polymers*; Ciferri, A., Ed.; Marcel Dekker: New York,: 2000; pp 263−321.
(24) Morkved, T. L.; Chapman, B. R.; Bates, F. S.; Lodge, T. P.; Stepanek, P.; Almdal, K. *Faraday Discuss.* **1999**, *(112)*, 335−350.
(25) Borukhov, I.; Leibler, L. *Macromolecules* **2002**, *35*, 5171−5182.
(26) Matsen, M. W. *Macromolecules* **1995**, *28*, 5765−5773.
(27) Tanaka, H.; Hashimoto, T. *Macromolecules* **1991**, *24*, 5713−5720.
(28) Tanaka, H.; Hashimoto, T. *Macromolecules* **1991**, *24*, 5398−5407.
(29) Zin, W. C.; Roe, R. J. *Macromolecules* **1984**, *17*, 183−188.
(30) Rangarajan, P.; Haisch, C. F.; Register, R. A.; Adamson, D. H.; Fetters, L. J. *Macromolecules* **1997**, *30*, 494−502.
(31) Olsen, B. D.; Jang, S. Y.; Luning, J. M.; Segalman, R. A. *Macromolecules* **2006**, *39*, 4469−4479.
(32) Lee, J. H.; Ruegg, M. L.; Balsara, N. P.; Zhu, Y. Q.; Gido, S. P.; Krishnamoorti, R.; Kim, M. H. *Macromolecules* **2003**, *36*, 6537−6548.
(33) Reference deleted in proof.
(34) Pryamitsyn, V.; Ganesan, V. *J. Chem. Phys.* **2004**, *120*, 5824−5838.
(35) Fredrickson, G. H.; Ganesan, V.; Drolet, F. *Macromolecules* **2002**, *35*, 16−39.
(36) Schmid, F. *J. Phys., Condens. Matter.* **1998**, *10*, 8105−8138.
(37) Matsen, M. W. *J. Phys., Condens. Matter.* **2002**, *14*, R21−R47.
(38) Drolet, F.; Fredrickson, G. H. *Phys. Rev. Lett.* **1999**, *83*, 4317−4320.

MA062876H